quenching ($k_q \sim 5 \times 10^8$ s^{-1} M^{-1}).[15,16]

2. Neither a direct excitation of molecular oxygen ($^3\Sigma_g^-O_2$) nor a $(O_2)_2$ simultaneous transition is responsible for the $^1\Delta_gO_2$ signal under our conditions.[10,17-20] Both cyclohexane and methanol can dissolve substantial amounts of oxygen[21] and exhibit oxygen-dependent absorption bands to the blue (<260 nm) of our pump wavelengths, but neither yield a $^1\Delta_gO_2$ signal when irradiated at 355 or 266 nm. It is expected that discrete oxygen transitions should be solvent independent. Furthermore, a plot of $^1\Delta_gO_2$ signal intensity (I_Δ) versus oxygen ($^3\Sigma_g^-O_2$) concentration shows no positive curvature for any of the solvents mentioned above. This eliminates the possibility of a $(O_2)_2$ simultaneous absorption.

3. The I_Δ is linearly dependent on the excitation laser energy. This precludes a multiphoton absorption in the solvent and the subsequent formation of $^1\Delta_gO_2$ in a trivial sensitized process.

4. The excitation wavelengths used in our experiments are to the red of the solvent $S_1 \leftarrow S_0$ transition. Therefore, in a single photon absorption, the singlet excited electronic states of the solvent are energetically inaccessible.

5. The $^1\Delta_gO_2$ is not produced by an adventitious sensitizer either present as an impurity in the solvent or one which is photolytically created. Upon prolonged irradiation, I_Δ is constant, and the absorption spectra of the irradiated samples show no evidence of degradation. For each solvent, we are able to observe a small absorbance under nitrogen-purged conditions at the excitation wavelength using a 10 cm path length cell. In the case of mesitylene, *p*-xylene, *o*-xylene, and 1,4-dioxane, this absorbance can be reduced by successive distillation, indicating the presence of impurities in our samples. However, the reduction in the absorbance upon distillation is not accompanied by an equal reduction in I_Δ. To further show that these impurities are not responsible for $^1\Delta_gO_2$ formation, we prepared standard benzene solutions of a known $^1\Delta_gO_2$ sensitizer, acridine, such that the solution optical density (OD) at 355 nm was comparable to that of the impurity as measured in a nitrogen purged solvent. Acridine in benzene is an efficient $^1\Delta_gO_2$ sensitizer (quantum yield = 0.8).[6] The I_Δ obtained by pumping the oxygen ($^3\Sigma_g^-O_2$) induced absorption bands in the aromatic solvents is at least three times greater than that observed for the standard acridine photosensitized $^1\Delta_gO_2$ signal. Although $^1\Delta_gO_2$ quantum yields of 2.0 are known, this phenomenon occurs at the limit of infinite oxygen concentration where all sensitizer singlet states are being quenched by $^3\Sigma_g^-O_2$.[6,22] At the oxygen concentrations used in our experiments, the results presented above indicate that if the impurity is indeed responsible for $^1\Delta_gO_2$ formation, it must have a $^1\Delta_gO_2$ quantum yield which far exceeds that of a standard photosensitized process.[6] Therefore, we conclude that $^1\Delta_gO_2$ is not produced by an adventitious sensitizer.

We suggest the observed $^1\Delta_gO_2$ will be formed primarily by a combination of two different channels: (1) a spin allowed, solvent–oxygen ($^3\Sigma_g^-O_2$) cooperative transition to a triplet charge transfer state[1] with subsequent intersystem crossing and dissociation to yield $^1\Delta_gO_2$ and the ground state solvent molecule and (2) an oxygen ($^3\Sigma_g^-O_2$) enhanced $T_1 \leftarrow S_0$ transition[2] followed by the sensitized formation of $^1\Delta_gO_2$ by the resulting triplet state. The wavelengths that correspond to the $T_1 \leftarrow S_0$ (0,0) absorption are as follows: benzene (340 nm),[2,23] toluene (346 nm),[24] *o*-xylene (348 nm),[24] *p*-xylene (355 nm),[24] and mesitylene (357 nm).[24] These distinct transitions are all found in the same spectral region as the broad, structureless Mulliken CT band. For benzene, toluene, and *o*-xylene, the excitation wavelength (355 nm)[5] is too far to the red to excite the $T_1 \leftarrow S_0$ transition. If the enhanced $T_1 \leftarrow S_0$ transition were the only channel responsible for the formation of the observed $^1\Delta_gO_2$, we would expect to see the $^1\Delta_gO_2$ signal only when *p*-xylene and mesitylene are pumped, and that the signal from *p*-xylene might be more intense than that from mesitylene. This is not the case. Rather, the I_Δ is linearly dependent on the OD of the oxygen-induced absorption at 355 nm for oxygenated benzene, toluene, *o*-xylene, and mesitylene. The *p*-xylene point, for which the $T_1 \leftarrow S_0$ transition is coincident with the excitation wavelength (355 nm), falls above the line, but I_Δ is not as large as that for mesitylene. Therefore, although some of the $^1\Delta_gO_2$ produced may be attributed to an oxygen-induced $T_1 \leftarrow S_0$ transition, we suggest that $^1\Delta_gO_2$ is also produced upon dissociation of a photolytically generated CT state.

In conclusion, we have provided direct spectroscopic evidence for the formation of $^1\Delta_gO_2$ subsequent to UV irradiation of a solvent–oxygen cooperative absorption band.

Acknowledgment. We thank Maria P. Dillon and Kai-Kong Iu for their assistance at various stages of this project. This work was supported by the National Science Foundation under Grant Number CHE-8501542.

(15) Wilkinson, F.; Brummer, J. G. *J. Phys. Chem. Ref. Data* **1981**, *10*, 809-999.
(16) A small amount of water was added to the solution in order to dissolve NaN_3.
(17) Rosenthal, I., in ref 10, pp 13-38 and references cited therein.
(18) (a) Eisenberg, W. C.; Taylor, K.; Veltman, J.; Murray, R. W. *J. Am. Chem. Soc.* **1982**, *104*, 1104-1105. (b) Eisenberg, W. C.; Snelson, A.; Butler, R.; Taylor, K.; Murray, R. W. *J. Photochem.* **1984**, *25*, 439-448.
(19) Koroll, G. W.; Singh, A. *Photochem. Photobiol.* **1978**, *28*, 611-613.
(20) Frei, H.; Pimentel, G. C. *J. Chem. Phys.* **1983**, *79*, 3307-3319.
(21) Battino, R., Ed. *IUPAC Solubility Data Series, Volume 7. Oxygen and Ozone*: Pergamon: Oxford, 1981; p 301.
(22) Dobrowolski, D. C.; Ogilby, P. R.; Foote, C. S. *J. Phys. Chem.* **1983**, *87*, 2261-2263.
(23) Sponer, H.; Kanda, Y.; Blackwell, L. A. *Spectrochim. Acta* **1960**, *16*, 1135-1147.
(24) Kanda, Y.; Shimada, R. *Spectrochim. Acta* **1961**, *17*, 279-285.

0002-7863/88/1510-0641$01.50/0

Use of $Ir_4(CO)_{11}$ To Measure the Lengths of Organic Molecules with a Scanning Transmission Electron Microscope

Frederic R. Furuya, Larry L. Miller,* J. F. Hainfeld, William C. Christopfel, and Peter W. Kenny

Department of Chemistry, University of Minnesota Minneapolis, Minnesota 55455
Biology Department, Brookhaven National Laboratory, Upton, New York 11973
Received September 21, 1987

We report an evaluation of the hypothesis that metal-cluster labels can be used to accurately measure molecular distances by transmission electron microscopy (TEM). Organic and most small biological molecules are essentially transparent in TEM, but distances between molecular sites can in principle be measured by attachment of electron-dense clusters to those sites. The present test utilized a sufficiently long and rigid organic spacer with specifically attached $Ir_4(CO)_{11}$ labels and took advantage of the capabilities of scanning transmission electron microscopy (STEM) for high resolution measurements on molecular materials. $Ir_4(CO)_{11}$-labeled molecules, which have not previously been used for TEM, are shown to be synthetically accessible, sufficiently stable, and immobile in the electron beam so that they may have wider TEM applicability.

Electron microscopists have had a long standing interest in labeling molecular structures with metals. In order to take advantage of the high resolution of modern microscopes and achieve specificity in imaging, attention has been given to metal clusters. Two types of clusters have been studied: anionic heteropolytungstates,[1,2] e.g., $(RC_5H_4)TiP_2W_{17}O_{61}^{7-}$, and cationic undecagold clusters,[3] e.g., $Au_{11}(CN)_3[P(C_6H_4CH_2NH_3^+)_3]_7$. Molecular

* Address correspondence to author at University of Minnesota.

(1) (a) Keana, J. F. W.; Ogan, M. D.; Lu, Y.; Beer, M.; Varkey, J. *J. Am. Chem. Soc.* **1985**, *107*, 6714. (b) Keana, J. F. W.; Ogan, M. D. *J. Am. Chem. Soc.* **1986**, *108*, 7951. (c) Keana, J. F. W.; Ogan, M. D.; Lu, Y.; Beer, M.; Varkey, J. *J. Am. Chem. Soc.* **1986**, *108*, 7956.
(2) Monson, K. L.; Wall, J. S.; Hainfeld, J. F. *Ultramicroscopy* **1987**, *21*, 147.
(3) (a) Safer, D.; Hainfeld, J. F.; Wall, J. S.; Riordan, J. *Science (Washington, D. C.)* **1982**, *218*, 290. (b) Frey, P. A.; et al. *Biochemistry* **1984**, *23*, 3849, 3857, 3863. (c) Safer, D.; Bolinger, L.; Leigh, J. S. *J. Inorg. Biochem.* **1986**, *26*, 77. (d) Lipka, J. J.; Hainfeld, J. F.; Wall, J. S. *J. Ultrastruct. Res.* **1983**, *84*, 120.

Scheme I[a]

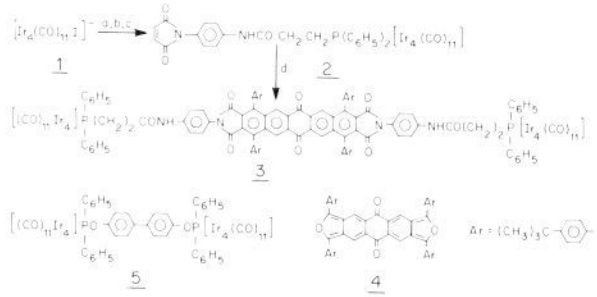

[a] (a) $(C_6H_5)_2PCH_2CH_2CO_2H$; THF, 24 h, room temperature (100%); (b) $(COCl)_2$, benzene/$CHCl_3$, 24 h, room temperature used without purification; (c) *N*-(*p*-aminophenyl)maleimide, $CHCl_3$, 2,6-di-*tert*-butylpyridine, 4 h, room temperature (79%); (d) **4**, $CHCl_3$, 18 h, room temperature, in the dark, followed by concentrated H_2SO_4 (28%).

separation distances have been measured between the four undecagold clusters which could be attached to avidin,[3a] and appropriately paired spots were observed from an organic compound to which two heteropolytungstates were attached.[1a] This observation was not analyzed in detail. Measurements of molecular distances are of interest to us for establishing the dimensions of molecular electronics structures, and it seemed important to more accurately test this TEM approach to distance measurement.

Et_4N^+, $[Ir_4(CO)_{11}I]^-$ (**1**), prepared[4] from commercial $Ir_4(CO)_{12}$, was employed to demonstrate the TEM qualities of tetrairidium clusters. Initial studies employed a conventional transmission electron microscope (Hitachi H-600, 100 kV) in the bright field mode. These studies gave evidence for good stability of the cluster in the beam and were preparatory for more thorough high resolution studies. With use of the Brookhaven STEM[5] which was operating at 40 kV, samples were subjected to a cumulative electron dose ranging from 5×10^4 to 4×10^5 e/nm^2. Specimen temperature was −135 °C during imaging. The sample was prepared by deposition from 10^{-6} M aqueous solution onto 25-Å carbon films. The dark field images showed bright spots ~6 Å in diameter. Computer analysis[5] indicated a mass of 800 ± 200 (sd) as expected for a single cluster. The Kolmogorov–Smirnov test applied to histograms from nine micrographs indicated a *random distribution of nearest neighbor distances.*

Our next goal was to obtain micrographs of a rigid molecule that had been cluster labeled on both ends. For this purpose, we prepared functionalized clusters like **2** taking advantage of the selective monosubstitution of phosphine for iodide,[4] not CO. The clusters were spaced apart by using synthetic methods that we have previously developed[6] for the preparation of long, yet soluble, molecular lines (Scheme I). The resulting compound **3**[7] has a rigid, linear spacer of 28 Å and flexible $COCH_2CH_2$ connectors. Importantly, **3** was soluble in organic solvents allowing purification, reliable assays of purity and structure, and application as a $CHCl_3$ solution to the carbon film substrate used for STEM. As anticipated, STEM micrographs (Figure 1A) showed paired 6-Å spots corresponding to individual molecules of **3**. The separations between 20 pairs were 20–37 Å ($\bar{x}$ = 27 ± 4 Å). This range covers virtually all of the conformations available to the flexible connectors and shows that individual molecules adopt a variety of conformations on the surface. More accurate distance measurements between rigidly placed sites on organic or biological molecules will require less flexible attachments than any of those previously employed.[2,3]

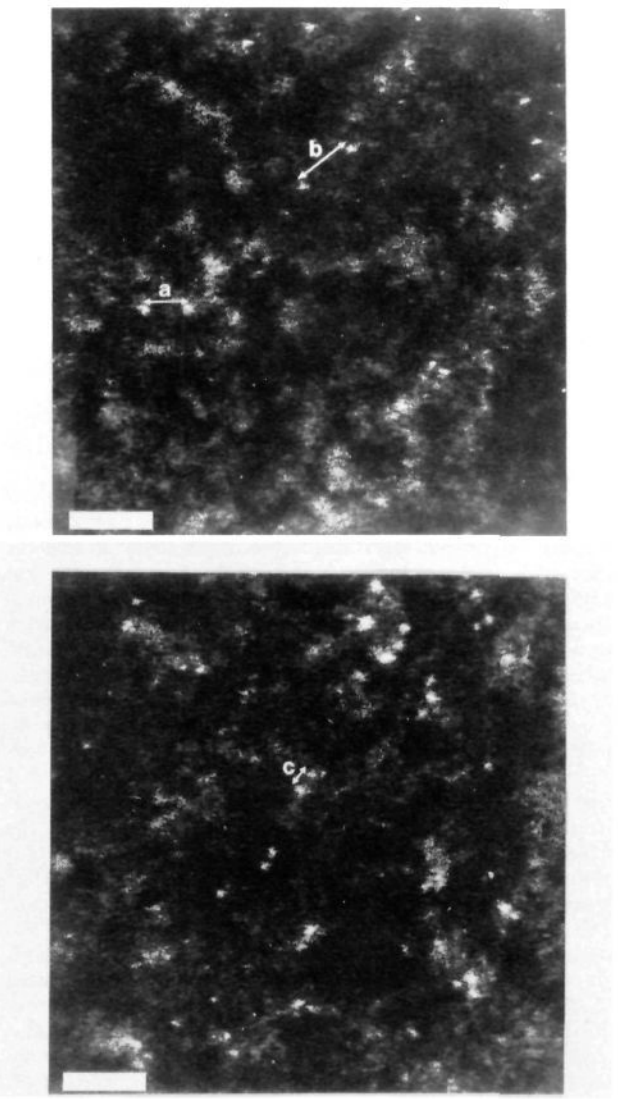

Figure 1. Dark field STEM images of **3** (A) (top) and **5** (B) (bottom). Dose 3.2×10^5 e/nm^2: (a) 26 Å, (b) 38 Å, (c) 10 Å. Bar = 50 Å.

A shorter bis cluster compound **5**[8] also gave 6-Å, paired spots (Figure 1B). The clusters were stationary in successive scans and did not damage substantially. Analysis of two typical micrographs containing 66 spots showed that 62 of them were correlated as pairs. The average separation for 100 pairs was 13 ± 4 Å. This affirms that the distances measured for **3** were not artifactual.

In summary, we have shown that small $Ir_4(CO)_{11}$ clusters are useful for STEM labelling; we have synthesized a linear spacer, attached the cluster to each end, and successfully correlated the cluster separation distances to those expected from molecular models. We expect that cluster labeling will allow us to measure the length of molecular lines on a surface, a measurement not currently feasible.

(4) Unpublished work of Roesselet and Gladfelter (Roesselet, K.; Gladfelter, W. University of Minnesota). Ros, R.; et al. *J. Chem. Soc., Dalton Trans.* **1986**, 2411.

(5) Mass analysis used the system described by Wall and Hainfeld (Wall, J. S.; Hainfeld, J. F.) *Ann. Rev. Biophys., Biophys. Chem.* **1986**, *15*, 355. Due to the high magnification (2×10^6), an extrapolated mass-per-unit-intensity calibration factor from tobacco mosaic virus was used. The radius of integration of 5 Å was chosen to account for possible misplacement of the center of integration.

(6) Christopfel, W. C.; Miller, L. L. *J. Org. Chem.* **1986**, *51*, 4169. Kenny, P. W.; Miller, L. L.; Chiba, T. *J. Org. Chem.* **1987**, *52*, 4327.

(7) Compound **3** (purified by preparative TLC on SiO_2 and then crystallization from toluene/CH_2Cl_2): ^{1}H NMR ($CDCl_3$) δ 8.96 (s, 4 H), 7.62–7.15 (m, 4 H), 2.91–2.77 (m, 4 H), 2.50–2.36 (m, 4 H), 1.43 (s, 36 H); IR (KBr) ν_{CO} cm^{-2} 2089, 2053, 2014, 1885, 1844, 1818, 177 average mass of the isotope envelope; $C_{130}H_{94}Ir_8N_4O_{30}P_2$ calcd (m + 1) 3791.9, obsd 3792.3.

(8) Compound **5** (4,4′-dihydroxybiphenyl plus $Cl(C_6H_5)_2P$, followed by reaction of the phosphinite product with **1** gave **5**): ^{1}H NMR ($CDCl_3$) δ 7.7–7.6 (m, 8 H), δ 7.6–7.4 (7, 12 H), δ 7.2–7.1 (m, 4 H), δ 6.8–6.7 (m, 4 H); IR (THF) ν_{CO} 2088 m, 2056 vs, 2035 m sh, 2020 s, 1847 m, 1826 m, cm^{-2}; MS, FAB calcd (M + 1) ($^{292}Ir_2$, $^{293}Ir_6$) 2709.7, obsd 2709.2; isotope cluster mass (M + 1) calcd 2706 (20), 2707 (69), 2708 (43), 2709 (100), 2710 (60), 2711 (93), 2712 (53), 2713 (53), obsd 2706 (32), 2707 (66) 2708 (73), 2709 (100), 2710 (76), 2711 (98), 2712 (56), 2713 (50).

Acknowledgment. This work was supported by the Office of Naval Research. We thank Grace G. Shiue for grid and E.M. sample preparation and Frank Kito and Martha Simon for STEM operation. Support for the STEM is provided by U.S.D.O.E., NIH Biotechnology Resource Grant RR01777, and NIH GM 31975.

The Equilibrium between $[CpCr(CO)_3]_2$ and $CpCr(CO)_3$. The Thermodynamics of Cr-Cr Single Bond Cleavage

Stephan J. McLain

Contribution No. 4246, Central Research & Development Department, Experimental Station E. I. du Pont de Nemours & Company Wilmington, Delaware 19898

Received May 26, 1987

There is NMR,[1] ESR,[2] and electrochemical[2] evidence for the reversible thermal dissociation of $[CpCr(CO)_3]_2$ in solution (reaction 1). We wish to report a quantitative study of this equi-

$$[CpCr(CO)_3]_2 \rightleftharpoons 2CpCr(CO)_3 \quad (1)$$
$$\mathbf{1} \qquad\qquad \mathbf{2}$$

librium which demonstrates that the equilibrium concentration of radical **2** is much higher than previously supposed. We also report the first infrared spectrum of **2** in solution.

Solutions of **1** have a strong UV absorbance that is associated with the Cr–Cr bond [λ_{max} = 450 nm, $^1(\sigma^2) \rightarrow {}^1(\sigma\sigma^*)$].[3,4] Upon dilution, this absorbance decreases more than expected from Beer's law behavior. If the diluted solution is reconcentrated, the original intensity of the 450-nm band is restored. Spectra recorded at different concentrations and scaled to adjust for concentration show an isosbestic point at 370 nm. These observations are consistent with a concentration dependent equilibrium between **1** and a species with no Cr–Cr bond.

The UV spectrum of **1** is temperature dependent. Increasing the temperature from −65 °C to +95 °C causes a reversible reduction in the intensity of the 450-nm band (Figure 1). This dramatic temperature dependence is consistent with the reversible formation of **2** (reaction 1). At temperatures below −35 °C, where the equilibrium is shifted entirely to **1**, the spectra have an isosbestic point at 456 nm (Figure 1 insert). The isosbestic behavior of **1** can be interpreted as a temperature dependent equilibrium between two rotational isomers with similar but not identical UV spectra (Figure 2).[1,5] $[CpMo(CO)_3]_2$, which is also known to be an equilibrium mixture of two rotomers,[6] exhibits similar isosbestic behavior (toluene solution, −35 °C to +45 °C, λ_{max} = 390 nm, isosestic point = 400 nm). The spectra shown in Figure 1 can be fit to the equilibrium model of reaction 1 to give accurate values of ΔH, ΔS, ϵ_1, and ϵ_2 (Table I).[7] Experiments in THF give similar results.

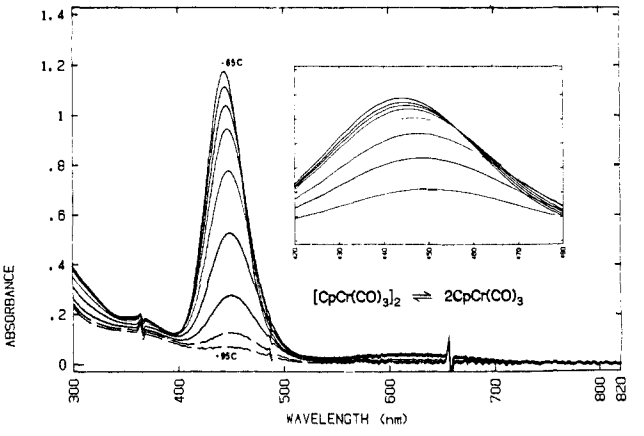

Figure 1. UV spectra of **1** in toluene (0.0020 M, 0.10 cm cell) from −65 °C to 95 °C (20 °C increments). Insert is −65 °C to 5 °C (10 °C increments). Spectra are corrected for the temperature dependence of the solvent density. The discontinuities at 360, 490, and 660 nm are artifacts.

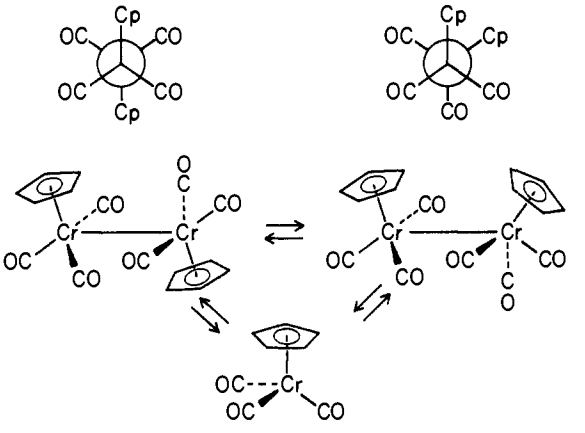

Figure 2. Equilibrium between anti dimer, gauche dimer, and monomer.

Table I. Thermodynamic Parameters[a] for the **1** ⇌ **2** Equilibrium

method	solvent	ΔH	ΔS	ΔG_{300}
UV[b]	toluene	15.8 (0.4)	37.1 (1.4)	4.6
IR	toluene			4.6
UV[c]	THF	14.8 (0.4)	34.3 (1.3)	4.5
IR	THF			4.7

[a] ΔH and ΔG in kcal mol^{-1}; ΔS in cal mol^{-1} K^{-1}; figures in parentheses are esd's. [b] ϵ_1 (456 nm) = 17 740 (960); ϵ_2 (456 nm) = 328 (106). [c] ϵ_1 (446 nm) = 18 600 (990); ϵ_2 (446 nm) = 180 (150).

IR spectra of **1** in solution show direct evidence of **2**. The complex solution spectrum of **1** has been attributed to an equilibrium mixture of anti and gauche rotometers (Figure 2, Figure 3a).[5] However, the concentration dependence of the spectrum (Figure 3a,b) can only be accounted for by an additional *intermolecular* equilibrium (i.e., reaction 1). Subtracting an appropriately scaled spectrum of a concentrated sample from the spectrum of a less concentrated sample gives a spectrum of **2**, the species favored at lower concentration (Figure 3c). This spectrum can be compared with the spectrum of **2** produced by photolysis of $CpCr(CO)_3H$ in a CO matrix (ν_{CO} = 1986, 1910, 1902 cm^{-1}).[8] The subtraction factor SF used to obtain Figure 3c can be used to calculate the equilibrium constant of reaction 1.[9] This value

(1) Adams, R. D.; Collins, D. E.; Cotton, F. A. *J. Am. Chem. Soc.* **1978**, *96*, 749–754.
(2) Madach, T.; Vahrenkamp, H. *Z. Naturforsch., B: Anorg. Chem., Org. Chem.* **1978**, *33*, 1301–1303.
(3) Madach, T.; Vahrenkamp, H. *Z. Naturforsch., B: Anorg. Chem., Org. Chem.* **1979**, *34*, 573–578.
(4) Meyer, T. J.; Caspar, J. V. *Chem. Rev.* **1985**, *85*, 187–218.
(5) Hackett, P.; O'Neill, P. S.; Manning, A. R. *J. Chem. Soc., Dalton Trans.* **1974**, 1625–1627.
(6) Adams, R. D.; Cotton, F. A. *Inorg. Chim. Acta* **1973**, *7*, 153–156.
(7) Starting with the definition of the equilibrium constant for reaction 1, $K_{eq} = [2]^2/[1]$, the following model was derived: absorbance = $\epsilon_1 l[1] + \epsilon_2 l[2]$; $[1] = \{[Cr_{tot}] - [2]\}/2$; $[2] = \{-K_{eq} + (K_{eq}^2 + 8K_{eq}[Cr_{tot}])^{1/2}\}/4$; $K_{eq} = e^{-\Delta G/RT}$; $\Delta G = \Delta H - T\Delta S$; $[Cr_{tot}] = \{[Cr_{25}]/d_{25}\}\{d_0 + AT_c + BT_c^2 + CT_c^3\}$ where ϵ_1, ϵ_2 = extinction coefficients of **1** and **2** at the isosbestic frequency; l = UV cell pathlength (cm); $[Cr_{tot}]$ = the total concentration of Cr atoms in solution; T, T_c = temperature in K and °C; $[Cr_{25}]$ = Cr atom concentration of the starting solution at 25 °C; d_0, d_{25} = solvent densities at 0 °C and 25 °C; A, B, C = solvent thermal expansion coefficients. The data were least-squares fit to this model by using SAS/ETS software with Gauss–Newton minimization.
(8) Mahmoud, K. A.; Rest, A. J.; Alt, H. G. *J. Chem. Soc., Chem. Commun.* **1983**, 1011–1013.
(9) The conditions for obtaining a null of **1** in a spectral substraction are $[1]_a - SF[1]_b = 0$. [1] can be expressed as a function of K_{eq} and $[Cr_{tot}]$: $[1] = \{4[Cr_{tot}] + K_{eq} - (8[Cr_{tot}]K_{eq} + K_{eq}^2)^{1/2}\}/8$. Substitution of this equation into the spectra subtraction equation gives an equation of the form $f(K_{eq}, [Cr_{tot}]_a, [Cr_{tot}]_b, SF) = 0$. The value if K_{eq} was determined by an iterative root finding program on a pocket calculator.

0002-7863/88/1510-0643$01.50/0